

Improved-confinement plasmas at high temperature and high beta in the MST RFP

This article has been downloaded from IOPscience. Please scroll down to see the full text article.

2009 Nucl. Fusion 49 104020

(<http://iopscience.iop.org/0029-5515/49/10/104020>)

View [the table of contents for this issue](#), or go to the [journal homepage](#) for more

Download details:

IP Address: 128.104.166.214

The article was downloaded on 14/10/2010 at 00:22

Please note that [terms and conditions apply](#).

Improved-confinement plasmas at high temperature and high beta in the MST RFP

B.E. Chapman¹, J.W. Ahn¹, A.F. Almagri¹, J.K. Anderson¹,
F. Bonomo², D.L. Brower³, D.R. Burke¹, K. Caspary¹,
D.J. Clayton¹, S.K. Combs⁴, W.A. Cox¹, D. Craig⁵, B.H. Deng³,
D.J. Den Hartog¹, W.X. Ding³, F. Ebrahimi¹, D.A. Ennis¹,
G. Fiksel¹, C.B. Forest¹, C.R. Foust⁴, P. Franz², S. Gangadhara¹,
J.A. Goetz¹, M.C. Kaufman¹, J.G. Kulpin¹, A. Kuritsyn¹,
R.M. Magee¹, M.C. Miller¹, V.V. Mirnov¹, P.D. Nonn¹,
R. O'Connell¹, S.P. Oliva¹, S.C. Prager¹, J.A. Reusch¹,
J.S. Sarff¹, H.D. Stephens¹, M.D. Wyman¹ and T. Yates³

¹ Department of Physics, University of Wisconsin, Madison, WI 53706, USA

² Consorzio RFX, 35127 Padova, Italy

³ Department of Electrical Engineering, University of California, Los Angeles, CA 90095, USA

⁴ Oak Ridge National Laboratory, Oak Ridge, TN 37831, USA

⁵ Wheaton College, Wheaton, IL 60187, USA

E-mail: bchapman@wisc.edu

Received 11 December 2008, accepted for publication 27 March 2009

Published 10 September 2009

Online at stacks.iop.org/NF/49/104020

Abstract

We have increased substantially the electron and ion temperatures, the electron density, and the total beta in plasmas with improved energy confinement in the Madison Symmetric Torus (MST). The improved confinement is achieved with a well-established current profile control technique for reduction of magnetic tearing and reconnection. A sustained ion temperature > 1 keV is achieved with intensified reconnection-based ion heating followed immediately by current profile control. In the same plasmas, the electron temperature reaches 2 keV, and the electron thermal diffusivity drops to about $2 \text{ m}^2 \text{ s}^{-1}$. The global energy confinement time is 12 ms. This and the reported temperatures are the largest values yet achieved in the reversed-field pinch (RFP). These results were attained at a density $\sim 10^{19} \text{ m}^{-3}$. By combining pellet injection with current profile control, the density has been quadrupled, and total beta has nearly doubled to a record value of about 26%. The Mercier criterion is exceeded in the plasma core, and both pressure-driven interchange and pressure-driven tearing modes are calculated to be linearly unstable, yet energy confinement is still improved. Transient momentum injection with biased probes reveals that global momentum transport is reduced with current profile control. Magnetic reconnection events drive rapid momentum transport related to large Maxwell and Reynolds stresses. Ion heating during reconnection events occurs globally, locally, or not at all, depending on which tearing modes are involved in the reconnection. To potentially augment inductive current profile control, we are conducting initial tests of current drive with lower-hybrid and electron-Bernstein waves.

PACS numbers: 52.55.-s, 52.55.Hc, 52.55.Tn

1. Introduction

The reversed-field pinch (RFP) is a toroidal magnetic fusion concept characterized by a relatively small toroidal magnetic field and large magnetic shear. The RFP is so named in part because the toroidal magnetic field is reversed in the edge

relative to its direction in the core. The large magnetic shear allows for a potentially large beta (plasma pressure normalized to the field pressure at the plasma boundary). However, the large shear also causes the RFP plasma to play host to a number of resonant tearing modes. The dominant modes have poloidal mode numbers $m = 1$ and $m = 0$. The $m = 1$ modes

are resonant at various locations in the plasma core, and the dominant modes are normally driven unstable by a gradient in the parallel current profile. The $m = 0$ modes are all resonant at the radius where the toroidal field reverses. In the Madison Symmetric Torus (MST) [1], the $m = 0$ modes are normally driven by nonlinear coupling with the $m = 1$ modes [2, 3]. The $m = 1$ and $m = 0$ modes reach their largest amplitude during magnetic reconnection events (or sawtooth crashes), which last for only about $100 \mu\text{s}$ but occur periodically in MST discharges. During reconnection events, and even between them, the $m = 1$ modes stochasticize the magnetic field in the core, leading to rapid transport of particles and energy [4, 5].

Nonlinear interaction of the $m = 1$ and $m = 0$ modes during reconnection events produces a number of powerful effects on the MST plasma. Two which will be described in this paper are intense ion heating and rapid momentum transport. The ion temperature increases several-fold due to a rapid conversion of stored magnetic energy to ion thermal energy, and the increase is global, due to the large number of reconnection sites (mode resonant surfaces) [6, 7]. We also observe ion heating localized to the toroidal field reversal radius in special cases where only $m = 0$ modes cause reconnection. Whether global or local, heating only occurs when the $m = 0$ modes are involved. Momentum transport also increases substantially during global reconnection events, causing a decrease in core plasma flow and an increase in the edge flow. Measurements in the edge reveal that fluctuation-induced Maxwell and Reynolds stresses are both large but of opposite sign, approximately balancing the measured change in plasma momentum [8]. Momentum transport is rapid even between reconnection events, as revealed in discharges where the plasma edge is accelerated with inserted biased probes. The core plasma spins up shortly thereafter, indicating rapid momentum transport. In plasmas with reconnection suppression, described in the next paragraph, the core plasma rotation exhibits essentially no change—momentum transport is substantially reduced.

In discharges in which reconnection is suppressed, we have now demonstrated a substantial increase in the electron and ion temperatures, the plasma density and the total beta. This has been achieved in part with an extension of reconnection suppression to a toroidal current of 0.5 MA, approaching MST's maximum current capability. Suppression of both the $m = 1$ and $m = 0$ tearing modes is achieved with a well-established technique for inductive control of the current profile [9, 10]. At relatively low toroidal plasma current, 0.2 MA, this has previously led to an electron temperature of 0.6 keV and a ten-fold improvement in the energy confinement time [10], producing tokamak-like confinement [11]. However, these discharges were limited by edge instability to a relatively low density $\sim 10^{19} \text{ m}^{-3}$. Given the small rate of electron-ion energy transfer, they were also limited to an ion temperature of about 0.2 keV [12]. The total beta reached a maximum of about 15%, but this was limited merely by the reduced ohmic heating power.

Now, at 0.5 MA and the usual low density, we have demonstrated plasmas with a central ion temperature $> 1 \text{ keV}$ and a central electron temperature of about 2 keV, both the largest temperatures achieved thus far in the RFP [13]. The large ion temperature is achieved with the intensification

of reconnection-based ion heating followed immediately by reconnection suppression and improved ion energy confinement. Electron energy confinement is simultaneously improved, leading to a rapid, ohmically driven increase in the electron temperature. The electron thermal diffusivity drops to about $2 \text{ m}^2 \text{ s}^{-1}$ near the reversal radius, and globally, the total (electron + ion) energy confinement time reaches 12 ms, also a record for the RFP.

In other discharges with current profile control, we have quadrupled the plasma density with injection of deuterium pellets [14, 15]. Core and edge fluctuations are reduced, energy confinement is improved and the ion temperature rises along with the electron temperature. The total beta is increased relative to that in low-density plasmas, ranging from 17% at 0.5 MA to 26% at 0.2 MA. In the highest beta plasmas, the central pressure gradient exceeds the Mercier criterion, and both pressure-driven interchange and pressure-driven tearing modes are calculated to be linearly unstable. Interchange modes have yet to be observed in these plasmas, but there is possible evidence of pressure-driven tearing.

With the goal of improving upon inductive control of the tearing modes, we are testing the feasibility of two rf techniques, one based on the lower-hybrid wave, the other based on the electron-Bernstein wave. The lower-hybrid system is already producing high-energy electrons, evidenced by the emission of hard x-rays with energies up to 50 keV [16]. The physics of electron-Bernstein wave injection is being established. Measurements indicate a potential coupling efficiency of up to 75% [17], and, from tests of low-power injection, the reflection coefficient can reach as low as 10%, in agreement with theory and computation [18].

The balance of this paper is organized as follows. We discuss reconnection and ion heating in section 2. Then in section 3 we describe the utilization of this heating to increase the ion temperature during subsequent reconnection suppression, and we discuss the simultaneous large increase in the electron temperature. The achievement and analysis of higher density, high-beta plasmas with pellet injection is the subject of section 4. Understanding and control of momentum transport is discussed in section 5, and results of rf feasibility tests are the subject of section 6.

2. Reconnection and ion heating

Particle acceleration and heating have been linked to magnetic reconnection in a wide variety of astrophysical, space and laboratory plasmas, but while the correlation is clear, the underlying physics has yet to be completely elucidated. In a number of RFP devices, including MST, reconnection has been cited as the cause of substantial ion heating [19–23]. In order to better understand the link between reconnection and ion heating, a charge-exchange-recombination spectroscopy (CHERS) diagnostic has been developed on MST to examine the evolution of the ion temperature profile during reconnection [6, 7]. As applied on MST, this diagnostic provides the temperature of fully stripped carbon ions at multiple radial locations (one location per discharge) with roughly 2 cm spatial resolution and a temporal resolution as fine as $10 \mu\text{s}$ [24]. Measurements of the ion temperature (T_i) profile during reconnection reveal that the

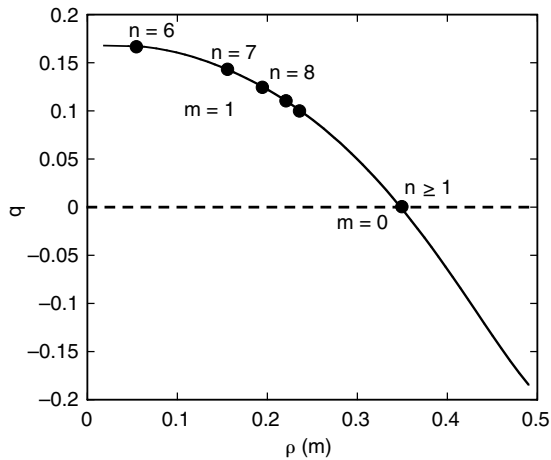


Figure 1. Profile of the safety factor in MST, showing the locations of the dominant $m = 1$ modes in the core and the $m = 0$ modes at the toroidal field reversal ($q = 0$) radius. Profile is from a plasma utilizing inductive current profile control. Boundary value of the safety factor is thus substantially more negative than in a typical RFP plasma. Profile reconstructed at 19.5 ms in shot 1070829100.

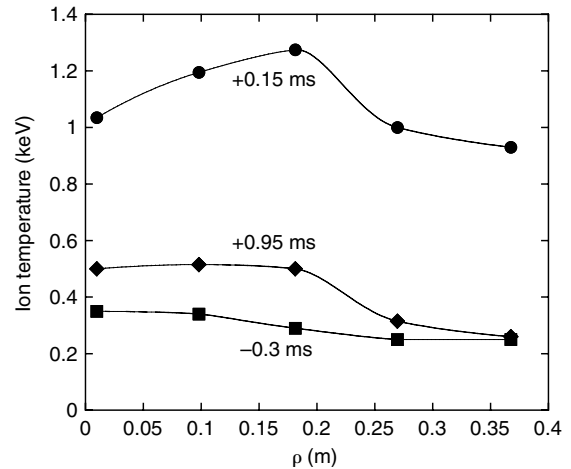


Figure 3. Ion temperature profiles measured at different times with respect to a large ensemble of global reconnection events occurring in discharges with a toroidal plasma current ~ 0.4 MA. The temperature reaches its maximum at +0.15 ms. Error bars (not shown) only slightly larger than the plot symbols.

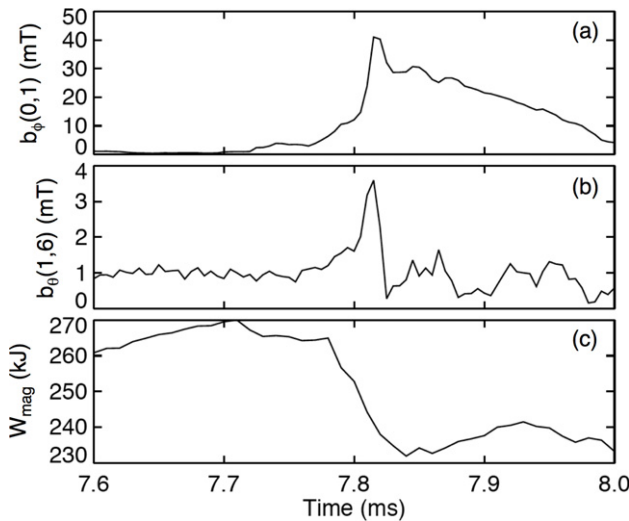


Figure 2. With a global reconnection event occurring at about 7.8 ms, temporal evolution of (a) $m = 0$, $n = 1$ tearing mode, (b) $m = 1$, $n = 6$ tearing mode and (c) volume-integrated stored magnetic energy. From shot 1070829100.

location and even the occurrence of heating depend on which modes, $m = 1$ and/or $m = 0$, are involved in the reconnection. It is also revealed that sudden, impulsive heating only occurs when reconnection is accompanied by a decrease in the internal stored magnetic energy.

The resonance locations of the $m = 1$ and $m = 0$ modes are shown in figure 1, which contains the safety factor profile from an MST discharge. The MST plasma has a major radius of 1.5 m and a minor radius of 0.5 m. The $m = 1$ modes have toroidal mode numbers $n = 6, 7, 8, \dots$, while the $m = 0$ modes have $n = 1, 2, 3, \dots$. During global reconnection events, all of the $m = 1$ and $m = 0$ mode amplitudes increase rapidly. The temporal evolution of the lowest- n , $m = 0$ and $m = 1$ modes during one such event is shown in figure 2. Here, the event occurs at about 7.8 ms. Another feature of global reconnection is a rapid drop in the stored magnetic energy (figure 2(c)). The

magnetic energy is estimated with a simple equilibrium model based on measurements of the magnetic field at the plasma boundary [25].

The temporal evolution of the T_i profile around global reconnection events in 0.4 MA MST discharges is shown in figure 3. These profiles are based on a large ensemble of similar events and are referenced to the relative time (0 ms) at which the tearing mode amplitudes peak [6, 7]. From shortly before to shortly after this peak, T_i increases to > 1 keV. Then, over about 1 ms, the T_i profile decays back toward its original shape and magnitude. This rate of decay in part reflects relatively poor ion energy confinement in these plasmas. The T_i profile at +0.15 ms exhibits an off-axis peak. This is consistent with the largest ion heating occurring where reconnection is most intense. The safety factor profile for the 0.4 MA plasmas in which these measurements were made [7] reveals that the $m = 1$, $n = 6$ resonant surface lies very close to the location of maximum T_i . This is the largest of the $m = 1$ modes during reconnection events.

The evolution of the T_i profile during two other types of reconnection event has also been examined in MST [6, 7]. One type is characterized by reconnection associated with only the $m = 0$ modes. In this case, ion heating is observed, but only in the vicinity of the $m = 0$ resonant surface. There is also a drop in the stored magnetic energy. The other type of reconnection event is characterized by activity in only the $m = 1$ modes. In this case, no ion heating is observed anywhere in the plasma, and there is no change in the magnetic energy. Hence, ion heating appears to require the involvement of the $m = 0$ tearing modes, and it is correlated with a decrease in magnetic energy. Magnetic energy has long been cited as a likely source of the ion heat.

3. Generation and capture of large T_i and T_e

We have now intensified the ion heating associated with global reconnection, and with reconnection suppression subsequent to the heating, we are able to maintain a large ion

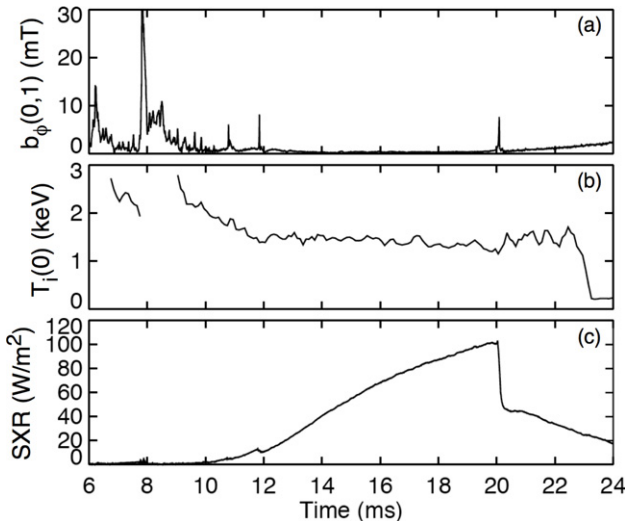


Figure 4. In a 0.5 MA discharge with inductive current profile modification beginning at 10 ms, time evolution of the (a) $m = 0$, $n = 1$ tearing mode, (b) central ion temperature and (c) central line-integrated x-ray emission. The apparent drop in ion temperature around 23 ms is an artefact of the diagnostic neutral beam termination. The reconnection event occurring just before 8 ms was described in detail in figure 2. Shot number 1070829100.

temperature [13]. An example of this is shown in figure 4, which contains data from a discharge with a toroidal plasma current of about 0.5 MA. Figure 4 contains the amplitude of the $m = 0$, $n = 1$ tearing mode, the central ion temperature measured with CHERS, and soft-x-ray emission measured through a $761 \mu\text{m}$ thick beryllium filter along a line of sight through the plasma centre. This x-ray emission increases with electron density, but the dominant contributor here is the electron temperature. From 10 to 20 ms, the line averaged density increases from 0.5×10^{19} to $0.85 \times 10^{19} \text{ m}^{-3}$. Occurring at around 6 and 8 ms in figure 4 are two global reconnection events. The latter event was described in detail in figure 2. The stored magnetic energy shown in figure 2 drops by an estimated 34 kJ ($\sim 13\%$) in about $60 \mu\text{s}$, implying a power greater than 500 MW. A fraction of this power is channelled to the impurity and majority ions. During the two events shown early in figure 4, the central T_i exceeds the upper range of the CHERS diagnostic, hence the gaps in the T_i data. However, T_i can be measured in the decay phase following each event, and these data imply that the central T_i may exceed 3 keV during heating. This is the largest ion temperature yet observed in the RFP, and it is achieved by simultaneously operating at large toroidal current and low density, and by increasing the degree of toroidal magnetic field reversal.

By simply increasing the toroidal current in MST, a larger temperature can be achieved during magnetic reconnection events. With an increase from 0.25 to 0.5 MA, the central temperature roughly triples, reaching 1.5 keV [7]. In addition to the toroidal current, the RFP equilibrium is also characterized by the so-called toroidal field reversal parameter, $F \equiv B_\phi(a)/\langle B_\phi \rangle$, where $B_\phi(a)$ is the toroidal field at the plasma boundary and $\langle B_\phi \rangle$ is the toroidal field averaged over the plasma cross section. In an RFP plasma, $F < 0$, and in MST, the degree of ion heating at reconnection events is also a strong function of F . In the discharge shown in

figure 4, F is about -0.25 between the large reconnection events. This corresponds to an edge safety factor, $q(a) = -0.05$. Otherwise similar discharges, even at high current, with F closer to zero exhibit much weaker heating. A similar relation between the reversal parameter and ion heating was also observed in the ZT-40M RFP [26]. Adjusting F to be more negative moves the $m = 0$ resonant surface further inside the plasma, and further away from the stabilizing influence of MST's thick conducting shell. This may facilitate more intense ion heating.

In addition to this change in equilibrium, low electron density is important. More negative F and low density leads to periods where magnetic fluctuations are spontaneously reduced, and global energy confinement is somewhat improved [27]. Two such periods, which are characterized in part by periodic small bursts of $m = 0$ mode activity, occur after the large events in figure 4. These periods often terminate with reconnection events having particularly large mode amplitudes. Relative to typical MST plasmas, the ion temperature in plasmas such as that in figure 4 decays more slowly following reconnection heating. This may result in part from somewhat improved ion energy confinement following the reconnection events.

The combination of intensified heating and slower temperature decay allows capture of substantial ion energy with reconnection suppression. In the discharge in figure 4, inductive modification of the current profile begins at 10 ms, leading to the eventual suppression of the $m = 0$ and $m = 1$ tearing modes, including the small bursts of $m = 0$ activity. This technique has been applied successfully in several RFP devices, but optimization continues [9, 10, 28–30]. The technique is based on a rampdown of the toroidal flux in the plasma, inducing a poloidal electric field to enhance the current flowing parallel to the edge magnetic field. Hence, F and $q(a)$ become much more negative. The q profile shown in figure 1, where $q(a) = -0.19$, was measured near the end of a period of toroidal flux rampdown.

The inductive programming applied here is similar to that previously described for MST [10, 12]. In 0.2 MA plasmas, this technique led to a tripling of T_e , reaching 0.6 keV, but T_i was unchanged at about 0.2 keV. Reconnection suppression in the 0.5 MA discharge shown in figure 4 results in a central $T_i > 1$ keV. The rate of temperature decay during this period is small, and this is due in part to increased ion energy confinement. The global ion energy confinement time is roughly estimated to increase ten-fold during reconnection suppression. This is based on a power balance calculation, including electron–ion heating and losses due to both charge exchange and convection. Charge exchange is one of the dominant channels of ion energy loss, and it is measured to drop roughly ten-fold. A substantial reduction is also observed in convection.

The period of reconnection suppression in figure 4 is interrupted briefly by a small burst of $m = 0$ activity near 20 ms. This is near the end of the poloidal current drive. After this burst, the low- n , $m = 0$ modes begin to increase slowly while most of the $m = 1$ modes remain fairly small. There is little apparent response in the central ion temperature. However, after having ramped up strongly with reconnection suppression, the central x-ray emission drops suddenly, dominantly reflecting a drop in the central T_e , and decays slowly thereafter.

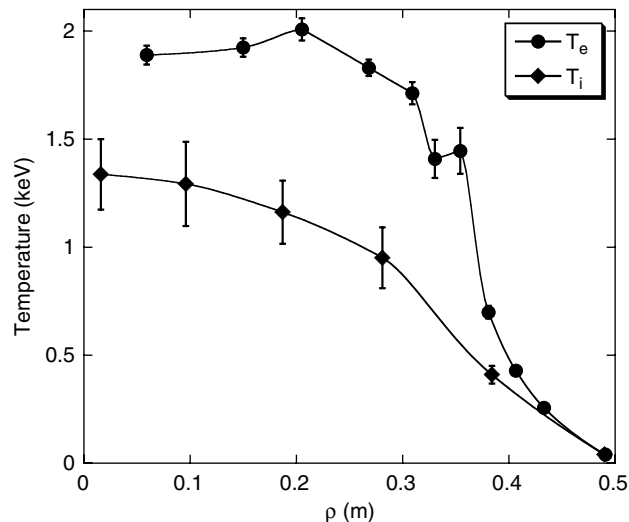


Figure 5. Electron temperature profile measured at 19.5 ms in the discharge shown in figure 4 and ion temperature profile compiled at 20 ms in a set of discharges similar to that in figure 4. Both profiles assume a boundary temperature of 40 eV.

Table 1. Improved-confinement plasma parameters with and without pellet injection at low and high toroidal plasma current. In the third row is the central line-averaged electron density normalized to the Greenwald density limit, defined in the text. Total beta is the volume-averaged pressure normalized to the total (toroidal + poloidal) magnetic field pressure at the plasma boundary. Data with pellets from [15]. Low-current data without pellets from [10]. High-current data without pellets from [13].

	w/o pellets	w pellets	w/o pellets	w pellets
I_ϕ (MA)	0.21	0.17	0.53	0.48
$n_e(0)$ (10^{19} m^{-3})	0.9	3.5	1.2	4.0
$\langle n_e \rangle / n_G$	0.26	1.2	0.13	0.66
P_{oh} (MW)	1.0	2.2	2.3	4.0
$T_e(0)$ (keV)	0.6	0.17	1.9	0.7
$T_i(0)$ (keV)	0.18	0.19	1.3	0.6
β_{tot} (%)	15	26	10	17
τ_E (ms)	10	>5	12	7

Profiles of T_e and T_i are shown in figure 5. The T_e profile was measured at 19.5 ms in the discharge shown in figure 4. This was possible with a new multi-point Thomson scattering diagnostic [31]. The T_i profile was compiled in discharges like that in figure 4, assembled from data at 20 ms, several majority-impurity-ion equilibration times after reconnection heating. With a Rutherford scattering diagnostic [32], the deuteron temperature was also measured at one location in these plasmas, confirming a large increase in the majority T_i . These central electron and ion temperatures represent substantial increases relative to what was achieved at 0.2 MA. These and other parameters are compared in table 1, in the two columns labelled ‘w/o pellets.’ In the present 0.5 MA plasmas, the combination of large ion and electron temperatures, along with a simultaneously reduced ohmic input power, results in a global energy confinement time of about 12 ms, a modest improvement over that achieved at 0.2 MA, and the largest yet achieved in the RFP.

Contributing to this global confinement improvement is a local reduction in the electron thermal diffusivity in the region $0.3 \text{ m} < \rho < 0.4 \text{ m}$, corresponding to steep gradients in the

T_e profile (figure 5). The diffusivity associated with the two steep gradients is about $2 \text{ m}^2 \text{ s}^{-1}$, likely the minimum value in the plasma. In the region $\rho > 0.4 \text{ m}$, the diffusivity increases monotonically out to the plasma boundary and is substantially larger than $2 \text{ m}^2 \text{ s}^{-1}$. The diffusivity in the region $\rho < 0.3 \text{ m}$ has yet to be determined, but the relatively flat T_e profile here implies that the diffusivity is probably larger than $2 \text{ m}^2 \text{ s}^{-1}$. Comparison of the T_e profile in figure 5 with the simultaneously measured q profile in figure 1 reveals that the steep T_e gradients lie on either side of the $q = 0$ surface. The local flattened region in the T_e profile is centred on the $q = 0$ surface, and the width of this region is consistent with that of an $m = 0$ island. The large gradients exist in a region of very small but finite q . The locally resonant $m = 1$ modes have toroidal mode numbers $n > 35$, and their respective adjacent resonant surfaces lie less than 1 mm apart. Hence, island overlap and stochasticity in this region is probable. The means by which electron thermal transport is reduced in this region remains to be determined. In addition to the large gradients in T_e , we note that the coarsely measured T_i profile also exhibits its largest gradient in the vicinity of $q = 0$.

4. Improved confinement at higher density and high beta

In plasmas fuelled with gas puffing and recycling, there is a soft density limit $\sim 10^{19} \text{ m}^{-3}$ for improved confinement [12]. Just above this limit, discrete bursts of $m = 0$ activity occur with regularity, and further above this limit, the $m = 0$ modes are continuously large. This activity limits the degree to which energy confinement can be improved. One result of this low-density restriction is the previous observation that T_i does not mimic the large increase observed in T_e . The characteristic time for transfer of energy from electrons to ions can range up to several hundred milliseconds in the hottest plasmas. This is far longer than the duration of the improved confinement. The large increase in T_e also halves the ohmic input power. Hence, while total beta increased with improved confinement, it was limited by the relatively small heating power.

Destabilization of the $m = 0$ modes with higher density is believed to result from the fact that gas puffing and recycling tend to deposit particles in the edge. We hypothesize that this causes unfavourable changes in the edge pressure and/or current gradient, thereby leading to $m = 0$ instability. This motivated the implementation of pellet injection on MST in order to deposit fuel directly in the core [14, 15].

An example of a discharge with pellet injection combined with inductive current profile control is shown in figure 6. The current profile modification begins at 10 ms, and two pellets arrive in the plasma shortly thereafter. The pellets more than triple the line-averaged electron density. Shown in figures 6(b) and (c) are the rms sums of magnetic fluctuations representing the behavior of the $m = 1$ and $m = 0$ modes. A few milliseconds after the pellets ablate, both $m = 1$ and $m = 0$ fluctuations are reduced. Note that pellet injection alone does not bring about fluctuation reduction. It merely provides a central source of fuel. With fluctuations reduced, both T_e and T_i increase, as shown in figure 6(d). These data were measured at $\rho = 0.1 \text{ m}$. The local electron temperature was measured with 2D x-ray tomography, based on the so-called double-foil

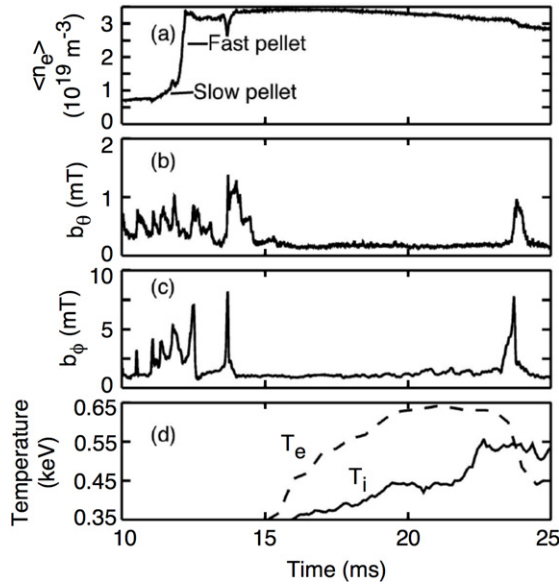


Figure 6. In a 0.5 MA discharge with two pellets injected just after the beginning (at 10 ms) of inductive current profile control, temporal waveforms of (a) the central line-averaged electron density, (b) $m = 1$, $n = 8$ –14 poloidal magnetic fluctuations, (c) $m = 0$, $n = 1$ –5 toroidal magnetic fluctuations and (d) the electron and ion temperature at $\rho = 0.1$ m (temperature data unavailable before 15 ms). Both pellets have a diameter of 1.6 mm. The fast and slow pellet speeds are, respectively, 1150 m s^{-1} and 167 m s^{-1} .

technique [33]. This is the first time that T_i has been observed to increase along with T_e during fluctuation reduction.

Pellet injection has been applied to both low- and high-current improved-confinement plasmas, allowing comparison with the results from improved-confinement at lower density. Some of the key parameters from these plasmas are shown in table 1. Recent work from the MST [15] and RFX-mod [34] experiments has demonstrated that the Greenwald density limit for tokamaks [35] applies to these two RFP devices as well. This limit on the line-averaged electron density $= I_{\phi}/\pi a^2$, where I_{ϕ} is the toroidal plasma current in megaamperes, a is the plasma minor radius in metres, and the density limit is in units of 10^{20} m^{-3} . In MST standard-confinement plasmas with and without pellet injection, premature termination of the discharge is observed when this limit is surpassed. The toroidal plasma current can drop to zero in as little as 5 ms. In table 1 we show line-averaged densities normalized to the Greenwald limit for improved-confinement plasmas. The low density MST discharges are well below the limit, but with pellet injection at low toroidal current, we are able to exceed the limit by 20% without premature discharge termination [15]. This is consistent with what is observed with pellet injection (central fuelling) in tokamak plasmas. At present on MST, the density with pellet injection at higher current is limited only by the size of the available pellets.

At both low and high current, the ohmic input power roughly doubles with pellet injection. This is due in large part to the facts that T_e is lower at high density, and the ohmic input power (and plasma resistivity) varies as $T_e^{-3/2}$. One reason for the smaller electron temperature with pellet injection is that the electron–ion energy transfer time decreases substantially, to as low as 5 ms. Hence, a substantial fraction of

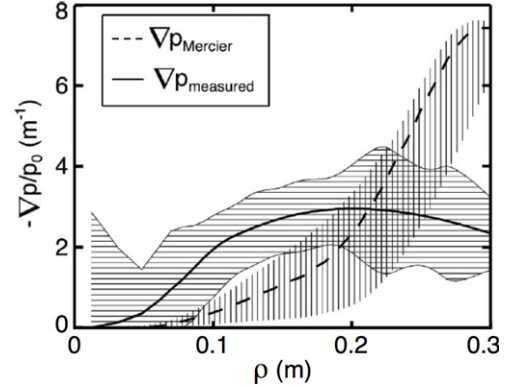


Figure 7. In a pellet-fuelled discharge with a total beta of 26%, profiles of the measured pressure gradient and the critical pressure gradient prescribed by the Mercier criterion. Profiles normalized to the central pressure. Shaded regions indicate estimated uncertainty.

the ohmic electron heat is transferred directly to the ions. This results in a substantial increase in the ion thermal energy. The energy confinement time with pellets is thus far not as large as that achieved without pellets. Nevertheless, the achieved confinement is much improved relative to the standard 1 ms, measured in plasmas without current profile control.

The larger stored thermal energy achieved with pellet injection has resulted in larger β_{tot} , with the largest value of 26% achieved at low current (table 1). This corresponds to a poloidal beta of 40%, normalizing to the poloidal magnetic field pressure at the plasma boundary, and a toroidal beta of about 100%, normalizing to the toroidal magnetic field pressure at the plasma boundary. These are the largest total and poloidal beta values achieved thus far in the improved-confinement RFP [14, 15]. The profile of the pressure gradient from one of these high-beta plasmas is shown in figure 7. Overlaid on this plot is the profile of the critical pressure gradient prescribed by the Mercier criterion, which when exceeded can theoretically lead to linearly unstable interchange modes. The criterion is expressed as

$$\frac{r B_{\phi}^2}{4\pi} \left(\frac{q'}{q} \right)^2 + 8p'(1 - q^2) > 0, \quad (1)$$

where q' is the radial derivative of the safety factor, representing magnetic field shear, and p' is the radial derivative of the pressure. The criterion weighs the destabilizing pressure gradient against the stabilizing magnetic field shear. In figure 7, this criterion is violated in the region $\rho < 0.2$ m.

Linear MHD computation with the DEBS code [36] has been applied to this high-beta equilibrium. The computation predicts that multiple pressure-driven interchange and tearing modes are linearly unstable. The interchange modes are radially localized modes with, e.g., $m = 3$, while the tearing modes are global with $m = 1$. As yet, we have not found evidence of interchange modes experimentally. This is similar to the case in some stellarator plasmas, where the Mercier criterion is exceeded with no indication of interchange instability [37]. However, there is potential experimental evidence for pressure-driven tearing in MST [14, 15]. Comparison of the $m = 1$ tearing mode spectra with current profile control at low density ($\beta_{\text{tot}} = 15\%$) and

high density ($\beta_{\text{tot}} = 26\%$) shows that the degree of fluctuation reduction is smaller in the larger beta plasmas. According to MHD computation, the usual current-gradient drive for these modes is essentially eliminated in both cases. The primary difference is that the pressure-gradient drive becomes significant with larger beta.

5. Understanding and control of momentum transport

The mechanism(s) underlying momentum transport in magnetic fusion plasmas continues to be an important line of research. Momentum transport has been examined in several scenarios in MST: during reconnection events and between reconnection events with and without current profile control. MST plasmas commonly exhibit spontaneous rotation, but this rotation is altered substantially and rapidly each time a global reconnection event occurs. The core plasma slows down, and the edge plasma spins up. The rate of momentum transport is roughly 1000 times faster than the classical rate. Previous work established the importance of the nonlinear $\mathbf{j} \times \mathbf{b}$ torque exerted between the core-resonant $m = 1$ modes and the edge-resonant $m = 0$ modes [38]. The core and edge are strongly coupled. Analogous to what was described earlier for ion heating, the $m = 0$ modes play a key role. In reconnection events involving only the $m = 1$ modes, there is no change in the momentum profile.

With a combination of internal measurements and MHD computation, we have improved substantially our understanding of momentum transport during global reconnection events [8]. The momentum balance equation for the MST plasma edge can be written as

$$\rho \frac{\partial \langle V_{\parallel} \rangle}{\partial t} \approx \langle \tilde{\mathbf{j}} \times \tilde{\mathbf{b}} \rangle_{\parallel} - \rho \langle \tilde{\mathbf{V}} \nabla \tilde{\mathbf{V}} \rangle_{\parallel}, \quad (2)$$

where ρ is the mass density, V is the plasma velocity, j is the current density, b is the magnetic field, tildes indicate fluctuating quantities and brackets indicate a flux-surface average. The term on the left is the ion inertia, while the terms on the right are the fluctuation-based Maxwell and Reynolds stresses. The temporal evolution of the terms in equation (2) over an ensemble of reconnection events is shown in figure 8. These terms were measured with a variety of probes inserted into the plasma edge. The data in figure 8 reveal that the two stresses are large but that they approximately balance each other. Their difference is roughly equal to the small ion inertia term. The data in figure 8 were measured near the $m = 0$ resonant surface. Away from this location in the plasma edge, the stresses are smaller but are still approximately balanced. Measurements with a laser Faraday rotation diagnostic of the Maxwell stress in the plasma core are consistent with what is observed in the edge. The Maxwell stress is much larger than the inertial term. The Reynolds stress in the core has yet to be measured.

These experimental observations are similar in many respects to recent findings from numerical simulations [39]. The simulations show that momentum transport is greatly enhanced in the presence of multiple tearing modes and that the nonlinear coupling of the modes is key—transport does not result merely from the superposition of independent, radially

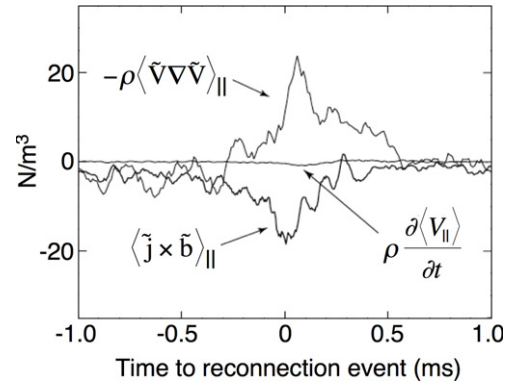


Figure 8. Temporal evolution of ion inertia and Reynolds and Maxwell stresses measured near the toroidal field reversal radius ($r/a = 0.83$) in a large ensemble of global reconnection events. Rapid oscillations indicate degree of experimental uncertainty.

separated effects. The nonlinear mode coupling leads to a phase change between the fluctuating quantities in the Maxwell and Reynolds stresses, thereby strengthening these turbulent stresses. Suppression of the $m = 0$ modes in the simulations leads to suppression of nonlinear coupling and momentum transport.

Global momentum transport between reconnection events has also been examined with an externally imposed alteration of the edge plasma rotation [40, 41]. This rotation is imposed with two positively biased probes inserted about 10 cm into the plasma. The probes are biased with respect to the MST vacuum vessel. This causes a radial current, which, combined with the dominantly poloidal edge magnetic field, leads to a toroidal torque. The effect of edge bias on the edge and core rotation in standard-confinement plasmas is shown in figure 9. Waveforms from plasmas without bias are also shown for reference. The edge rotation is represented by the toroidal velocity of C III ions, while the core rotation is represented by the phase velocity of the $m = 1, n = 6$ tearing mode. Shortly after the bias current is turned on, the edge velocity increases rapidly to a steady value, and the core rotation begins increasing at about the same time. This implies fairly strong coupling between the core and edge plasma, and the rate of momentum transport is roughly 100 times faster than the classical prediction. When bias is applied to discharges with inductive current profile control and fluctuation reduction, the responses of both the edge and core rotation are substantially different (figure 10). The edge plasma responds more rapidly to the applied bias current and reaches a larger velocity, but there is little comparable response in the core. This implies that the edge and core are more effectively isolated.

6. Testing the feasibility of rf current drive on MST

While inductive modification of the current profile has proven a robust means of reducing magnetic fluctuations and improving energy confinement, the technique is inherently transient, and relatively crude, in that it does not allow precise tailoring of the current profile. This has motivated the development of techniques to noninductively and more precisely alter the current profile. One possible means to this end is the application of rf. Feasibility studies of two rf techniques are

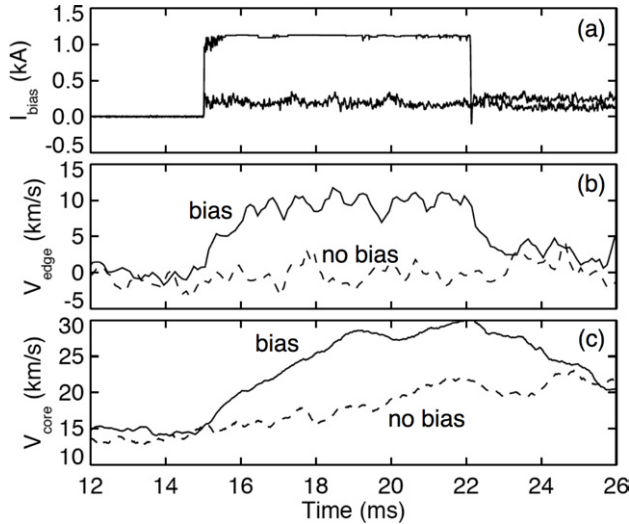


Figure 9. In 0.2 MA standard-confinement plasmas with two positively biased probes inserted 10 cm into the plasma, (a) combined bias current carried by the two probes, (b) edge toroidal flow velocity, represented by the velocity of C_{III} ions and (c) core toroidal flow velocity, represented by the phase velocity of the $m = 1, n = 6$ tearing mode. In the no-bias case, biasing probes are inserted but grounded. All data based on an ensemble average of similar discharges.

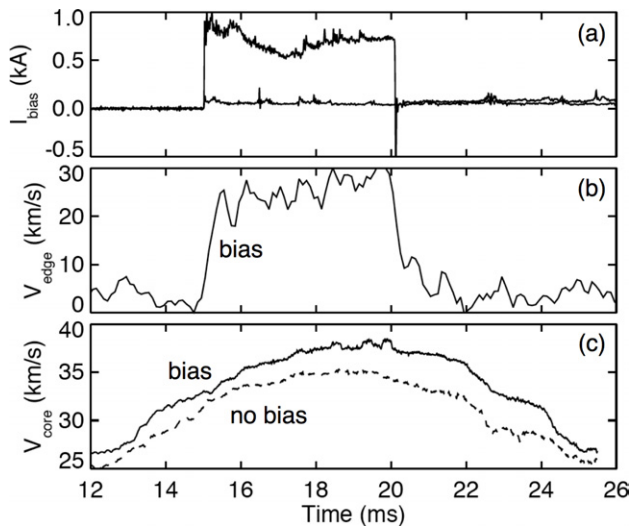


Figure 10. In 0.2 MA improved-confinement plasmas with inductive current profile control beginning at 10 ms, same setup and signals as shown in figure 9. The C_{III} velocity was unavailable for the no-bias plasmas, but the estimated majority ion rotation in similar plasmas shows that the edge rotation remains small, as in figure 9.

presently underway on MST, the first tests of rf in the RFP. The techniques are based on the injection of lower-hybrid waves (LHW) and electron-Bernstein waves (EBW). These two approaches have complementary strengths and challenges. The physics and application of current drive with LHW is well established on tokamaks, but antenna design for MST has required substantial innovative engineering. On the other hand, the EBW approach benefits from a relatively simpler antenna design, but EBW physics is not yet well established for a high-beta plasma like the RFP.

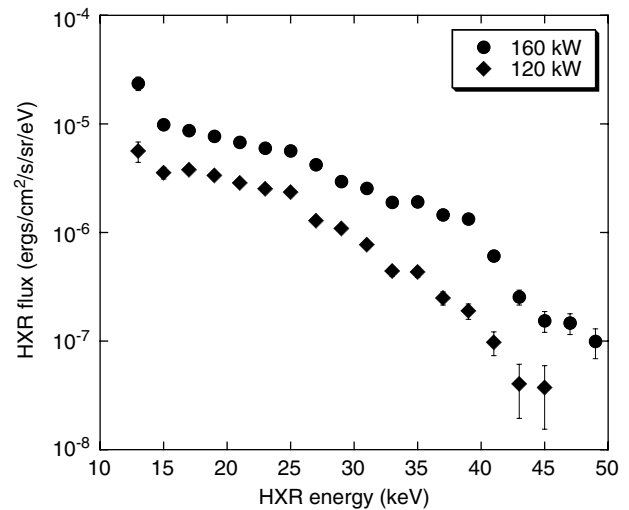


Figure 11. Spectra of hard-x-ray photons measured near lower-hybrid antenna at two input powers.

The design of the LHW antenna for MST is tightly constrained by the MST vacuum vessel. Large portholes are disallowed to avoid overly large magnetic error fields. The rather large antenna must therefore be mounted on the interior surface of the vessel. This constrains the height (or radial extent) of the antenna to avoid having the antenna act as a limiter. These and other constraints forced a design based on a novel interdigital line antenna [42]. This is a travelling-wave antenna which in MST operates at 800 MHz with an $n_{||} \sim 7.5$, parameters dictated by modelling to drive current predominantly in the edge region ($r/a \sim 0.8$) with strong single-pass absorption. One encouraging LHW result thus far is the emission of hard-x-ray photons with energies up to 50 keV, demonstrating that there are electrons with at least this energy in the plasma [16]. The flux of hard x-rays is also found to increase with the power applied to the antenna. Hard-x-ray energy spectra for two applied power levels are shown in figure 11. At present, this emission exhibits a degree of toroidal localization. Depending on the direction of LHW injection, hard x-rays are detected over a toroidal extent of up to 120° , roughly centred on the antenna.

Given the relatively large beta of the RFP, the electron cyclotron resonance is inaccessible for current drive. This is in contrast to the tokamak where electron cyclotron current drive and heating are staples. The EBW is a nearly electrostatic solution of the hot plasma dielectric tensor and presents a potential alternate route for use of the electron cyclotron resonance [43]. Theory, simulations and experiments show that the EBW converts to and from an electromagnetic wave at the extreme edge, but practical use of this conversion requires low reflected power and high conversion efficiency. As an initial step in testing the feasibility of EBW injection, a compact waveguide antenna was installed on an existing MST porthole to study coupling at low rf power (< 10 W) [18]. Full-wave coupling theory was incorporated into a simulation and tested against experiment. The simulation predicted that the reflected power should depend strongly on the edge density gradient at the upper hybrid resonance (typically within 1–2 cm of the antenna). This result was thoroughly tested with experimental measurements, as shown in figure 12. The

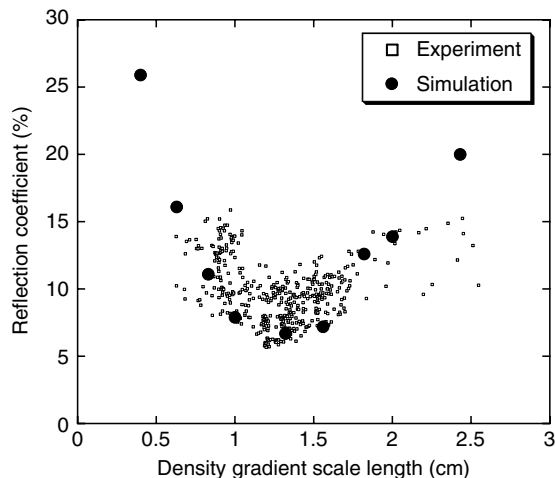


Figure 12. Comparison of experimental and simulated reflection coefficients for a range of density gradient scale lengths in front of the EBW antenna. Plot symbols for experimental data reduced for plot clarity.

measured and predicted reflection coefficients agree well over a range of density scale lengths typical of the MST edge, and the data show that the reflection coefficient can be as low as 10%. Blackbody levels of cyclotron emission from the plasma core have also been measured, and the associated mode conversion was measured to have an efficiency of about 75% [17]. Reciprocity then implies that EBW injection from the edge has the potential to drive current efficiently in the plasma.

7. Summary and conclusions

In low-density, high-current MST plasmas, we have now demonstrated improved confinement of hot thermal ions with $T_i > 1$ keV and hot thermal electrons with $T_e \sim 2$ keV. This is in addition to previously reported good confinement of 20 keV beam-injected fast ions [44] and 100 keV runaway electrons [45]. We have demonstrated inductive control of the dominant tearing modes over almost all of MST's range of toroidal plasma current. The achievable density during improved confinement has quadrupled, in one case exceeding the Greenwald density limit, and beta has been increased to the point that we are challenging two pressure-driven stability limits. The ultimate beta limit in the RFP has yet to be determined, but we conclude that pressure-gradient-driven tearing modes may play an important role. We have also improved our understanding of ion heating and momentum transport due to reconnection, showing, e.g. that the $m = 0$ modes play a critical role in both processes. The identified importance of the Reynolds and Maxwell stresses during reconnection events, when magnetic fluctuations and magnetic self-organization are dominant, may have relevance to particular plasma regimes in other fusion devices, such as the tokamak. Two potential examples are recently achieved plasmas with induced edge stochasticity and plasmas nearing disruption.

Motivated by these results and by the need for even further improvements in MST's performance, we are testing the feasibility of current profile control with two rf techniques.

Several upgrades to MST's control systems are also underway. A simple upgrade to the pellet injector has already provided substantially larger pellets and larger plasma density. A relatively high-power tangential neutral beam will be installed to augment ohmic heating and contribute to the search for a beta limit. MST's toroidal field power supply, formerly consisting of several discrete, inflexible capacitor banks, will be supplanted by a fully programmable solid-state system. This will allow attempts at further optimization of inductive current profile control with a wide variety of toroidal field waveforms.

Two of the outstanding questions from this work are (1) the ultimate degree to which ion heat can be generated and captured by control of reconnection and (2) whether or not this technique could actually be useful in a fusion reactor. Previous measurements in MST showed a tripling of the ion temperature with an increase in the toroidal plasma current from 0.25 to 0.5 MA [7]. An RFP reactor is expected to require a toroidal plasma current of at least 10 MA, suggesting the possibility of substantially larger ion heating at a reactor-relevant current. However, these reconnection events engender rapid electron energy loss, causing a decrease in the electron temperature, and, at present, the most energetic reconnection events require relatively low density. Hence, it remains to be determined how the relative advantages and disadvantages of this technique balance out.

Acknowledgments

This work was made possible by the unwavering support of the entire MST team and by the US Department of Energy and the National Science Foundation.

References

- [1] Dexter R.N., Kerst D.W., Lovell T.W., Prager S.C. and Sprott J.C. 1991 *Fusion Technol.* **19** 131
- [2] Assadi S., Prager S.C. and Sidikman K.L. 1992 *Phys. Rev. Lett.* **69** 281
- [3] Choi S., Craig D., Ebrahimi F. and Prager S.C. 2006 *Phys. Rev. Lett.* **96** 145004
- [4] Fiksel G., Prager S.C., Shen W. and Stoneking M. 1994 *Phys. Rev. Lett.* **72** 1028
- [5] Biewer T.M. *et al* 2003 *Phys. Rev. Lett.* **91** 045004
- [6] Gangadhara S., Craig D., Ennis D.A., Den Hartog D.J., Fiksel G. and Prager S.C. 2007 *Phys. Rev. Lett.* **98** 075001
- [7] Gangadhara S., Craig D., Ennis D.A., Den Hartog D.J., Fiksel G. and Prager S.C. 2008 *Phys. Plasmas* **15** 056121
- [8] Kuritsyn A., Fiksel G., Almagri A.F., Brower D.L., Ding W.X., Miller M.C., Mirnov V.V., Prager S.C. and Sarff J.S. 2009 Measurements of the momentum and current transport from tearing instability in the MST reversed-field pinch *Phys. Plasmas* submitted
- [9] Sarff J.S., Hokin S.A., Ji H., Prager S.C. and Sovinec C.R. 1994 *Phys. Rev. Lett.* **72** 3670
- [10] Chapman B.E. *et al* 2001 *Phys. Rev. Lett.* **87** 205001
- [11] Sarff J.S. *et al* 2003 *Nucl. Fusion* **43** 1684
- [12] Chapman B.E. *et al* 2002 *Phys. Plasmas* **9** 2061
- [13] Chapman B.E. *et al* 2009 Generation and confinement of hot ions and electrons in a reversed-field pinch plasma *Phys. Rev. Lett.* in preparation
- [14] Wyman M.D. *et al* 2008 *Phys. Plasmas* **15** 010701
- [15] Wyman M.D. *et al* 2009 *Nucl. Fusion* **49** 015003

- [16] Kaufman M.C. *et al* 2007 *Proc. 17th Topical Conf. on Radio Frequency Power in Plasmas (Clearwater, FL)* vol 933 p 309 <http://www.ornl.gov/sci/fed/rf2007/>
- [17] Chattopadhyay P.K., Anderson J.K., Biewer T.M., Craig D., Forest C.B., Harvey R.W. and Smirnov A.P. 2002 *Phys. Plasmas* **9** 752
- [18] Cengher M., Anderson J.K., Svidzinski V. and Forest C.B. 2006 *Nucl. Fusion* **46** 521
- [19] Howell R.B. and Nagayama Y. 1985 *Phys. Fluids* **28** 743
- [20] Carolan P.G. *et al* 1987 *Proc. 14th European Conf. on Controlled Fusion and Plasma Physics (Madrid, Spain)* vol 2 (Petit-Laney: European Physical Society) p 469
- [21] Fujisawa A., Ji H., Yamagishi K., Shinohara S., Toyama H. and Miyamoto K. 1991 *Nucl. Fusion* **31** 1443
- [22] Scime E., Hokin S., Mattor N. and Watts C. 1992 *Phys. Rev. Lett.* **68** 2165
- [23] Horling P., Hedinz G., Brzozowskiz J.H., Tennforsz E. and Mazur S. 1996 *Plasma Phys. Control. Fusion* **38** 1725
- [24] Den Hartog D.J. *et al* 2006 *Rev. Sci. Instrum.* **77** 10F122
- [25] Antoni V., Merlin D., Ortolani S. and Paccagnella R. 1986 *Nucl. Fusion* **26** 1711
- [26] Wurden G.A. *et al* 1988 *Proc. 15th European Conf. on Controlled Fusion and Plasma Physics (Dubrovnik, Croatia)* (Petit-Laney: European Physical Society) p 533
- [27] Chapman B.E., Chiang C.-S., Prager S.C., Sarff J.S. and Stoneking M.R. 1998 *Phys. Rev. Lett.* **80** 2137
- [28] Bartiromo R., Martin P., Martini S., Bolzonella T., Canton A., Innocente P., Marrelli L., Murari A. and Pasqualotto R. 1999 *Phys. Rev. Lett.* **82** 1462
- [29] Yagi Y., Maejima Y., Sakakita H., Hirano Y., Koguchi H., Shimada T. and Sekine S. 2002 *Plasma Phys. Control. Fusion* **44** 335
- [30] Cecconello M., Malmberg J.-A., Spizzo G., Chapman B.E., Gravestjin R.M., Franz P., Piovesan P., Martin P. and Drake J.R. 2004 *Plasma Phys. Control. Fusion* **46** 145
- [31] Reusch J.A., Borchardt M.T., Den Hartog D.J., Falkowski A.F., Holly D.J., O'Connell R. and Stephens H.D. 2008 *Rev. Sci. Instrum.* **79** 10E733
- [32] Reardon J.C., Fiksel G., Forest C.B., Abdrashitov A.F., Davydenko V.I., Ivanov A.A., Korepanov S.A., Murachtin S.V. and Shulzhenko G.I. 2001 *Rev. Sci. Instrum.* **72** 598
- [33] Franz P. *et al* 2006 *Rev. Sci. Instrum.* **77** 10F318
- [34] Puiatti M.E. *et al* 2009 *Phys. Plasmas* **16** 012505
- [35] Greenwald M. *et al* 1988 *Nucl. Fusion* **28** 2199
- [36] Schnack D.D., Barnes D.C., Mikic Z., Harned D.S. and Caramana E.J. 1987 *J. Comput. Phys.* **70** 330
- [37] Okamura S. *et al* 1995 *Proc. 15th Int. Conf. on Plasma Physics and Controlled Nuclear Fusion Research (Seville, Spain, 1994)* vol 1 (Vienna: IAEA) p 381
- [38] Hansen A.K., Almagri A.F., Craig D., Den Hartog D.J., Hegna C.C., Prager S.C. and Sarff J.S. 2000 *Phys. Rev. Lett.* **85** 3408
- [39] Ebrahimi F., Mirmov V.V., Prager S.C. and Sovinec C.R. 2007 *Phys. Rev. Lett.* **99** 075003
- [40] Almagri A.F., Chapman J.T., Chiang C.-S., Craig D., Den Hartog D.J., Hegna C.C. and Prager S.C. 1998 *Phys. Plasmas* **5** 3982
- [41] Kuritsyn A. 2008 *Bull. Am. Phys. Soc.* **53** 120
- [42] Goetz J.A. *et al* 2001 *Proc. 14th Topical Conf. on Radio Frequency Power in Plasmas (Oxnard, CA)* vol 595 p 253 http://aries.ucsd.edu/mau/RF2001_old/
- [43] Forest C.B., Chattopadhyay P., Harvey R.W. and Smirnov A.P. 2000 *Phys. Plasmas* **7** 1352
- [44] Fiksel G., Hudson B., Den Hartog D.J., Magee R.M., O'Connell R., Prager S.C., Beklemishev A.D., Davydenko V.I., Ivanov A.A. and Tsidulko Y.A. 2005 *Phys. Rev. Lett.* **95** 125001
- [45] O'Connell R. *et al* 2003 *Phys. Rev. Lett.* **91** 045002